Research Article

Anika Brahm*, Edgar Reetz, Simon Schindwolf, Martin Correns, Peter Kühmstedt and Gunther Notni

3D shape measurement with thermal pattern projection

DOI 10.1515/aot-2016-0052
Received September 22, 2016; accepted November 8, 2016

Abstract: Structured light projection techniques are well-established optical methods for contactless and nondestructive three-dimensional (3D) measurements. Most systems operate in the visible wavelength range (VIS) due to commercially available projection and detection technology. For example, the 3D reconstruction can be done with a stereo-vision setup by finding corresponding pixels in both cameras followed by triangulation. Problems occur, if the properties of object materials disturb the measurements, which are based on the measurement of diffuse light reflections. For example, there are existing materials in the VIS range that are too transparent, translucent, high absorbent, or reflective and cannot be recorded properly. To overcome these challenges, we present an alternative thermal approach that operates in the infrared (IR) region of the electromagnetic spectrum. For this purpose, we used two cooled mid-wave (MWIR) cameras (3–5 µm) to detect emitted heat patterns, which were introduced by a CO_2 laser. We present a thermal 3D system based on a GOBO (GOes Before Optics) wheel projection unit and first 3D analyses for different system parameters and samples. We also show a second alternative approach based on an incoherent (heat) source, to overcome typical disadvantages of high-power laser-based systems, such as industrial health and safety considerations, as well as high investment costs. Thus, materials like glass or fiber-reinforced composites can be measured contactless and without the need of additional paintings.

Keywords: infrared imaging; thermal imaging; thermal pattern projection; three-dimensional shape measurement.

OCIS code: 110.3080 infrared imaging; 120.3940 metrology; 120.4820 optical systems; 110.6820 thermal imaging; 150.6910 three-dimensional sensing.

1 Introduction

Structured light projection techniques for three-dimensional (3D) surface measurements have become increasingly attractive for a wide range of industrial and academic applications through the advantages of an optical and nondestructive measurement technique [1]. Since the early years of optical 3D measurements, the research focuses on improvement of accuracy, resolution, and speed [2]. Impressive high-speed measurements of moving objects or fast scenes have been presented. New projection techniques, such as laser speckles [3] or aperiodic sinusoidal fringes that are generated with GOBO (GOes Before Optics) systems [4] exceed the limits of conventional projection techniques up to 3D frame rates of multiple kHz.

Certainly, the performance of 3D systems depends, besides technical and mechanical parameters, especially on the optical properties of the objects and surfaces to be measured. In the visible wavelength range (VIS), many materials with transparent, reflective, high-absorbent, or translucent properties exist, for example, glass, crystals, plastics, and fiber-reinforced composites. Those materials affect the measurements drastically or even make them impossible in relation to the measurement principle based on diffuse light reflection. Often, coatings are used to overcome these issues, but they are not practicable in all cases because their application is time consuming for inline

***Corresponding author: Anika Brahm,** Fraunhofer Institute for Applied Optics and Precision Engineering (IOF), Albert-Einstein-Str. 7, 07745 Jena, Germany, e-mail: anika.brahm@iof.fraunhofer.de
Edgar Reetz and Martin Correns: Department of Mechanical Engineering, Industrial Image Processing, Technical University Ilmenau, 98693 Ilmenau, Germany
Simon Schindwolf and Peter Kühmstedt: Fraunhofer Institute for Applied Optics and Precision Engineering (IOF), Albert-Einstein-Str. 7, 07745 Jena, Germany
Gunther Notni: Fraunhofer Institute for Applied Optics and Precision Engineering (IOF), Albert-Einstein-Str. 7, 07745 Jena, Germany; and Department of Mechanical Engineering, Industrial Image Processing, Technical University Ilmenau, 98693 Ilmenau, Germany

processes, and they often cannot be removed without residue. One approach can be an error simulation [5] for the corrections or improvement of measurement results in a post-process. Unfortunately, they are still time consuming and require prior knowledge about the samples or the measurement setup in some cases. An overview of further techniques of specular or transparent objects is given in Ihrke et al. [6].

To overcome the optical challenges in the visible wavelength range, we present another approach that is partially based on the 'scanning from heating (SFH)' method. It operates in the thermal infrared region of the electromagnetic spectrum and was first demonstrated by Eren et al. [7] at which they measured transparent plastics and glass. They used a laser scanning system as heat source and generated heating points on the objects' surfaces. Thermal cameras where used to observe the emitted heat information to reconstruct the surfaces. Almost the same procedure was shown by Aubreton et al. [8] who measured different metallic geometries with high-power lasers up to the kW range. Nevertheless, the measurement areas and speed of acquisition was limited by the method of pointwise scanning. Thus, a different approach for faster application is needed. Furthermore, there are existing applications where a laser source should be avoided.

In Ref. [9], a first demonstrator system was shown based on a CO_2 laser with a single thermal camera and phase-shifting projection technique of sinusoidal heat patterns. In contrast, we reported about two different techniques in Ref. [10] where we showed for the first time two promising projection techniques based on aperiodic sinusoidal patterns generated by a freeform mirror and a metallic GOBO wheel to overcome the hurdles of fast acquisition. We used a stereo-vision setup of two uncooled long-wave infrared (LWIR) cameras and showed the limitations of these measurements at 3D reconstructed surfaces of glass and fiber-reinforced plastics. Now, we will show the first results of an optimized acquisition technique. Here, we used mid-wave infrared (MWIR) cameras instead of LWIR cameras because of laser safety reasons through their spectral sensitivity of 3–5 µm and better thermal sensitivity with less than 20 mK instead of 75 mK.

Furthermore, we present an alternative approach based on incoherent light sources. In contrast to the GOBO setup, the incoherent setup is the other way around. The light source emits in the mid-wave infrared range, while the detector is a typical LWIR focal plane array microbolometer with a spectral sensitivity between 7.5 and 13 µm. To avoid damaging the detector, the light source does not meet the sensitivity range of the detector.

Section 2 presents a short description of our thermal simulation model and results, which can be used for further assessments of thermal 3D system designs. In section 3, we show our experimental results of a thermal 3D GOBO system. It operates with a CO_2 laser as a coherent source for the generation of a heat pattern and two MWIR cameras in a stereo-vision setup. In section 4, we present an alternative approach, which avoids the classical laser approach and uses an incoherent heat source. Finally, we will conclude in section 5.

2 Theoretical background

2.1 Thermal simulation

We solved the heat equation and generated a simulation to estimate required parameters such as projection duration or intensity of a heat source (e.g. CO_2 laser) for an arbitrary temperature contrast on the object surfaces [11]:

$$\rho(u)\cdot c(u)\cdot\frac{\partial u}{\partial t}=\vec{\nabla}(k(u)\cdot\vec{\nabla}u)+\dot{q}=\frac{\partial k(u)}{\partial u}\cdot(\vec{\nabla}u)^2+k(u)\cdot\Delta u+\dot{q} \tag{1}$$

(ρ… mass density, c… heat capacity, k… thermal conductivity, u… temperature, $\vec{\nabla}$… gradient, Δ… Laplace operator, $\dot{q}$… flow of heat energy, which is caused by the heat sources).

We assumed only a small temperature difference of less than 1 K for short-projection durations and to avoid destructive effects on the measurement objects. Thus, we neglected the temperature dependence of the material parameters. Then, equation is read:

$$\rho\cdot c\cdot\frac{\partial u}{\partial t}=k\cdot\Delta u+\dot{q} \tag{2}$$

As heat source, we used a CO_2 laser with a Gaussian intensity profile:

$$I(r,z)=\frac{2\cdot P}{\pi w_r^{\,2}(z)}\cdot\exp\left(-\frac{2r^2}{w_r^{\,2}(z)}\right) \tag{3}$$

(r… radius, z… depth, P… beam power, w_r… beam waist)

We solved equation (2) with some boundary conditions, which are explained more in detail in Ref. [10]. With these conditions and the method of finite elements, the heat equation has been solved numerically for different materials and system parameters. We verified the simulations with different materials such as glasses and plastics,

Table 1: Laser power (W), which is needed to heat up borofloat® glass 33 to 0.5 K.

Diameter of measurement area (mm)	Laser duration (s)			
	0.1	0.3	0.5	1
150	41.8 W	24.1 W	18.7 W	13.4 W
300	167.2 W	96.6 W	74.9 W	53.2 W
500	464.4 W	268.2 W	208.0 W	148.4 W

Table 2: Laser power (W), which is needed to heat up borofloat® glass 33 to 1 K.

Diameter of measurement area (mm)	Laser duration (s)			
	0.1	0.3	0.5	1
150	85.6 W	49.6 W	37.6 W	26.4 W
300	342.4 W	198.4 W	150.0 W	105.6 W
500	951.1 W	551.2 W	418.0 W	293.3 W

different projection durations, and intensities of the CO_2 laser. The results were proofed with measurements. Thus, it is possible to estimate certain parameters for a proposed thermal 3D system. For example, Tables 1 and 2 show simulated values for the laser power of our laser system that is needed to heat up the surface of a borofloat® glass 33 (thickness 3 mm) by 0.5 and 1 K, respectively. Further, the results can be transferred to estimations with real heat patterns, too.

2.2 Basic setup

The basic setup of our thermal 3D stereo-vision system is shown in Figure 1. First, a heat pattern is projected and absorbed on the object surface due to the fact that a few materials lost their transparency in the infrared region of the electromagnetic spectrum. Then, both cameras measure the emitted heat radiation from the object surface simultaneously. According to the time delay between the projection and acquisition, the contrast and sharpness of the heat pattern can change. Similar to the 3D measurements in visible range, a stack of multiple 2D heat pattern images will be reconstructed based on a calibrated system. In Ref. [10], the calibration technique is described more in detail, but depends in principle on Refs. [12] and [13]. Further, the reconstruction is done by finding corresponding pixels in both cameras followed by triangulation [14].

3 GOBO system with laser-induced heat pattern

3.1 Measurement setup with MWIR cameras

Figure 2 shows the experimental setup of our 3D system. We used a CO_2 laser at 10.6 µm and 80 W output power for the generation of a heat pattern. Protected gold mirrors reflect the laser beam into a telescope of zinc selenide (ZnSe) lenses (first lens: f = 15 mm, second lens: f = 254 mm) to expand the beam up to a diameter of about 45 mm. A GOBO wheel (described in [15]) and made of steel operates as a mask to project an aperiodic sinusoidal pattern in combination with a CO_2 laser illumination. A third ZnSe lens (f = 127 mm) projects the aperiodic binary fringes onto the measurement area with a diameter of about 150 mm at a distance of about 550 mm. The GOBO wheel can be rotated by a stepper motor to change the projection pattern.

Two cryogenic-cooled MWIR cameras (3–5 µm) of type FLIR A6753sc with a resolution of 640 × 512 pixels, full frame rate of 120 Hz, and sensitivity less than 20 mK were arranged in a distance of about 190 mm and triangulation angle of 26.5°. The resolution in the measurement plane was about 0.24 mm.

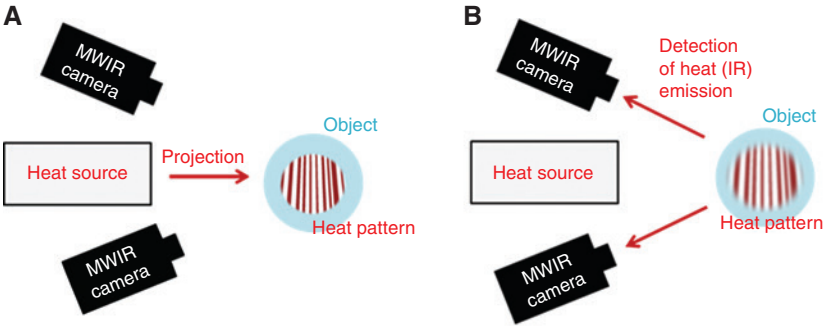

Figure 1: Setup of a thermal 3D stereo-vision system: (A) heating process; (B) measurement process.

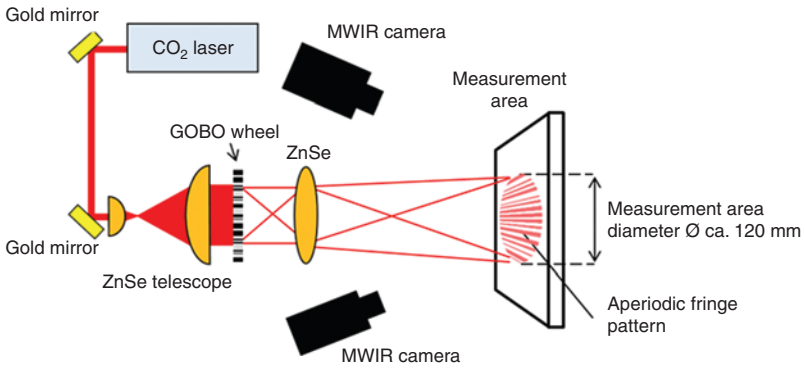

Figure 2: Experimental setup.

Usually, uncooled LWIR cameras are much cheaper than cooled MWIR cameras. But in contrast to the measurements with LWIR cameras in Ref. [10], no external or internal shutter against the laser radiation at 10.6 µm is needed anymore because of their different spectral sensitivity and lens materials. Thus, one important restriction of the measurement speed can be removed with the change of the camera system. Other good points are better thermal sensitivities and higher repetition rates of cooled cameras (e.g. FLIR model X6900sc with a full frame rate up to 1000 Hz) because of cooled photonic sensors instead of microbolometer technology.

3.2 Measurement results

The thermal 3D measurement principle is similar to that in Ref. [10], where we showed first the reconstruction results of materials like glass and CRFP. The objects were radiated with a certain exposure time and both LWIR cameras measured the emitted heat pattern simultaneously.

This time, we used MWIR cameras. In total, 10 projection images per MWIR camera were taken for one 3D reconstructed surface, whereas we used a time delay of a few seconds between each exposure step to avoid the influence of a heating effect of the object.

For an evaluation of the new thermal 3D system, we determined the flatness measurement error of a natural hard rock surface plate made of granite as quality parameter. The actual flatness measurement error of this granite plate is defined with less than 6 µm. On this, we calculated the standard deviations of the measured 3D points, which were fitted to plane. For initial analyzes, we varied only three parameters. The influence of (1) the rotation of the GOBO wheel, (2) the thermal contrast depending on the image acquisition over the heating process, and (3) the exposure time.

1. We used a constant exposure time of 200 ms of the CO_2 laser and varied the rotation. We measured the heating process over the time and extracted only the projection images with the maximum thermal contrasts (about 0.35 K). An example is shown in Figure 3A, which was achieved immediately after the heating process of 200 ms. Then, we reconstructed the surface of the granite plate for five different step widths of the motor and extracted the standard deviations

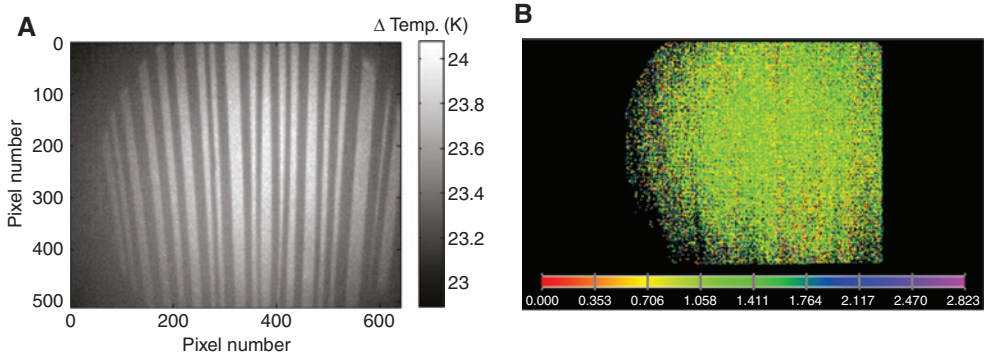

Figure 3: Thermal image (A) of the granite plate, which was taken directly after the heating process; (B) reconstructed 3D point cloud with a color-coded height profile in mm.

of the 3D points. An example of such a reconstructed surface with a color-coded height profile is shown in Figure 3B.

The step width of the stepper motor varies the rotation of the GOBO wheel. Here, the minimum step width of the stepper motor was limited to 0.028°. Thus, the motor steps were calculated into certain rotations of the stripes where we calculated with the period of the middle stripe width (2.7 mm). We defined the rotation by a full period (black and white stripes) as 100% for comparability reasons of such a GOBO wheel with wheels of different middle stripe widths. At 50%, the GOBO wheel was moved only by have a period of the middle stripe width. Figure 4 shows the results. Because of the noise of the thermal imaging cameras (about ±0.15 K was measured), the flatness errors of the 3D points show higher values than the optimized 3D systems, which operate in the visible wavelength range [16]. Further, the manufacturing process of this wheel was limited to a minimum stripe width of about 250 µm and, thus, is too large for the recommended number of periods in the measurement area (compare [14]) up to now.

Nevertheless, a trend to lower flatness errors can be observed by reducing the rotational movement of the GOBO wheel. Less than 20% rotation was not possible with this wheel because of its weight and the limitations due to the stepper motor. This leaves optimization possibilities for future experiments with different parameters, e.g. exposure time, dimension, and rotation of the GOBO wheel, etc.

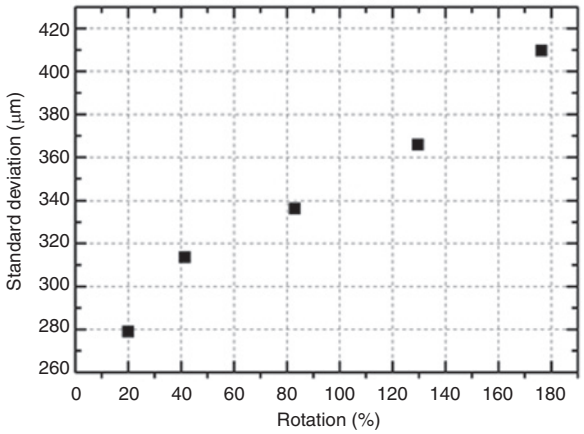

Figure 4: Flatness error of the measured 3D point clouds in correlation to the rotation of the GOBO wheel: A rotation of 100% corresponds to a movement by a full period (dark and white) of the middle stripe width.

2. In Figure 5A, a typical heating process is shown where we measured the temperature contrast of the heat pattern in the middle of the granite plate for an exposure time of 200 ms. We averaged the temperature values to about two regions (dark and white) of 9 pixels in the middle of the plate and subtracted their mean values from each other. It can be seen that the temperature contrast increases as long as the radiation is in progress and, then, drops down with an exponential decay due to the process of thermal diffusion. Furthermore, we used a constant rotation of 20% and reconstructed the surface at five different moments over this heating process. Again, the flatness errors were determined by the standard deviations of the measured 3D points, which were fitted to a plane. Figure 5B shows the results at 40 ms ($\Delta T = 0.18$ K), 140 ms ($\Delta T = 0.3$ K), 200 ms ($\Delta T = 0.4$ K), 500 ms ($\Delta T = 0.2$ K), and 1 s ($\Delta T = 0.1$ K). As expected, the minimal flatness

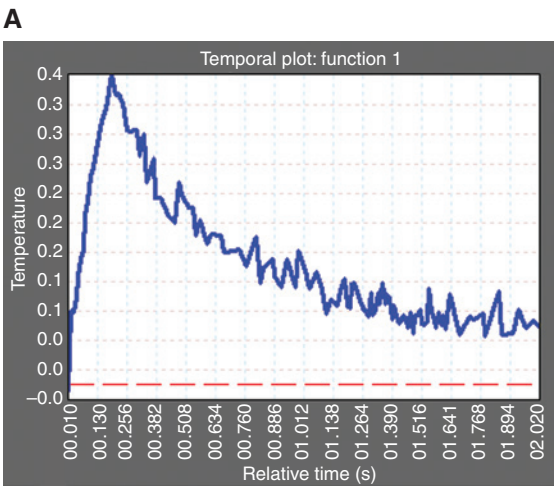

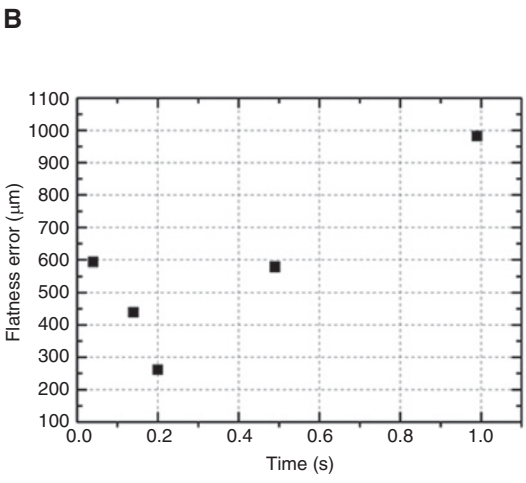

Figure 5: (A) Temperature differences are a heating process; (B) flatness error at certain time positions during the heating process.

error is achieved when the temperature contrast of the pattern arrives at its maximum. Certainly, this effect has to be verified by further measurements with other exposure times and with respect to a possible limit.

3. In the third experiment, we varied the parameter of the exposure time. The rotation was readjusted to 20%, and the projection images were reconstructed at their maximum temperature contrasts immediately after each exposure time. To avoid too many simultaneous parameters during this experiment, a cooling time of a minute has been introduced between each measurement.

The results are shown in Figure 6. Owing to a longer exposure time, the temperature contrast of the stripes increases linearly. This was expected, as a time of cooling was observed during each measurement. In contrast, the flatness error decreases with higher temperature contrasts in the images. This even leads to a flatness error of about 150 µm at 500-ms exposure time, which also demonstrates optimization possibilities in future. However, it can be assumed that there will be a compromise between a fast and accurate measurement. In further experiments, we will analyze the effect of thermal diffusion and temperature contrasts as we avoid cooling times during the image acquisition to speed up the measurements and find out the limits.

The following measurement examples demonstrate the impressive potential of this new technology (see Figure 7). We measured and reconstructed the surface of a transparent plastics cylinder (A, B), transparent glass bottle (C, D), and a strong reflective fiber composite (E, F) with the GOBO system. Depending on the material parameters, the exposure time was varied between 100 ms and 500 ms.

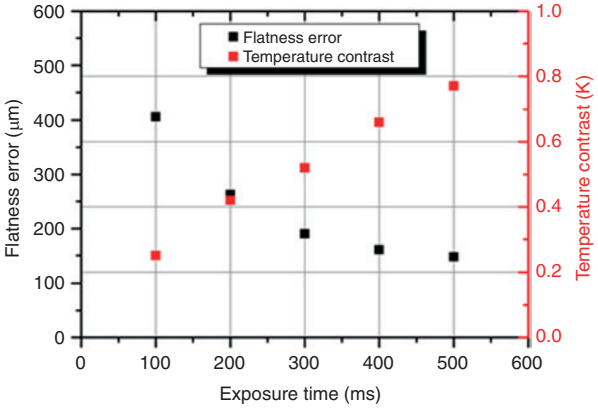

Figure 6: Flatness errors and temperature contrasts depending on the exposure time.

4 Incoherent heat radiation

The laser-based setup provides many benefits, especially a very short measurement time due to the high-energy density of the laser beam. However, that also could be a disadvantage, e.g. when an 80-W laser power is in contrast to safety and health regulations in human-machine interaction workplaces and areas. As the high-speed setup is also a high-cost setup, the idea of the incoherent radiation setup was to build a low-risk and low-budget system.

Heating technology, in general, is divided by the energy source into thermal convection, mechanical deformation, and electric current and electromagnetic radiation. The 3D restoration process is based on structured pattern projection. Therefore, an omnidirectional/indirect energy source is not suitable. Electromagnetic radiation sources, especially infrared energy sources, fit the task, as long as the beam could be utilized for pattern projection and is nondestructive to the measuring object.

In a thermal radiator, the absolute power radiated mainly depends on two factors: the area and the temperature. Another constraint for the setup is to avoid interferences with or influencing the detector wavelength range. According to the black body curve, this means that increasing the temperature increases the total energy emitted, but the peak wavelength decreases. For an experimental setup, that means that the wavelength is as short as possible for the objects to be examined, and the area is structurally designed as large as possible to image the pattern. For black plastic and CFRP, the wavelength is not critical because they absorb over a wide wavelength range. Another important parameter for the experimental setup is the thermal inertia of the radiator, so the time constants for heating and cooling (response time) should be as short as possible. Quartz glass heater and ceramic heater have a long response time. Their emission could interfere with the detector range, and their power density per area was not sufficient for the experimental setup. With the combination of the parameters explained above, the decision was in favor of a carbon-filament lamp. The lamp, the so-called ‘golden 8 twin-tube’ emitter with a backside gold coating, directs as much energy as possible to the metal pattern mask.

As already mentioned, the radiating surface is an important aspect. For the projection system, this means that the optical system must have large dimensions. Accordingly, lenses are required that have relatively large diameters and a transmissions range that fits the source

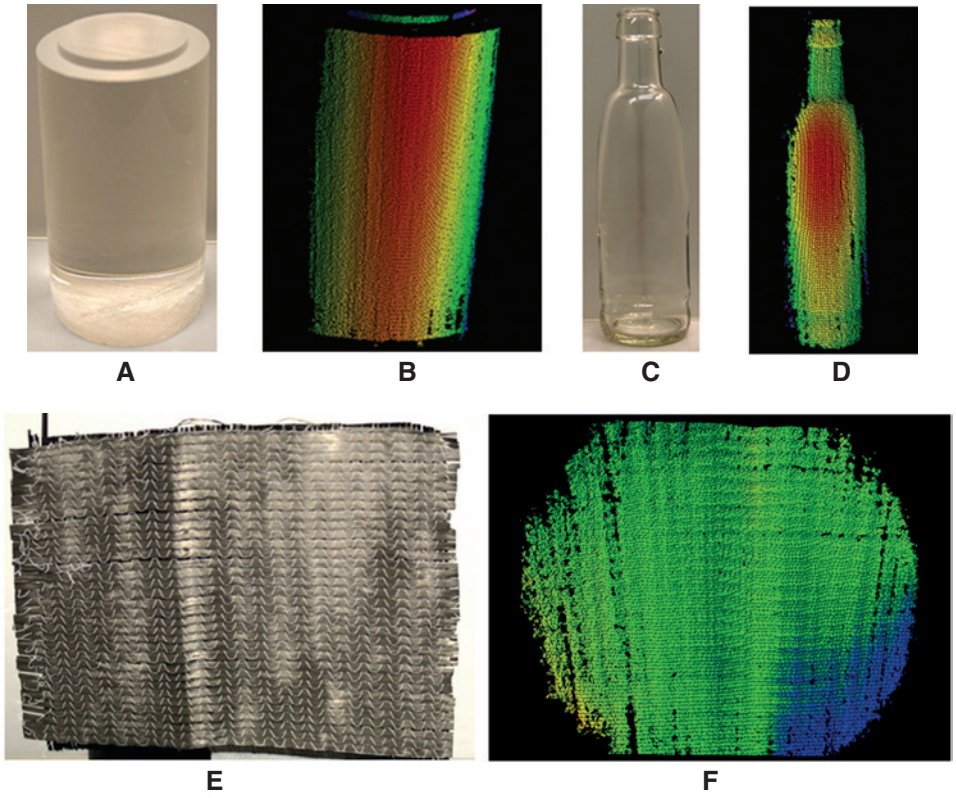

Figure 7: Measurement examples and corresponding color-coded 3D point clouds – (A, B) transparent plastic cylinder; (C, D) glass bottle; and (E, F) fiber composite.

emission range. Therefore, a silicon lens with a 120-mm total diameter was chosen for the experimental setup. The carbon filament temperature is around 1200°C when running and has an emission maximum around 2 µm. The lamp has a response time of about 2–3 s and provides 110 kW/m^2.

For the setup, a common uncooled microbolometer focal plane array camera was used, employed with 320×256 pixels returning a 14-bit depth signal at 60 Hz (FLIR A35). The microbolometer sensitivity is around 50 mK and provides a detection range between 7.5 and 13 µm. The experimental setup is displayed in Figure 8.

Owing to the setup properties, the image quality cannot be as good as is with the GOBO setup. For transparent plastics like PMMA or CFRP, the relative contrast ratio that this setup can produce seems good enough. In Figure 9, a screenshot from the camera video stream is shown. Four regions of interest (roi) with different

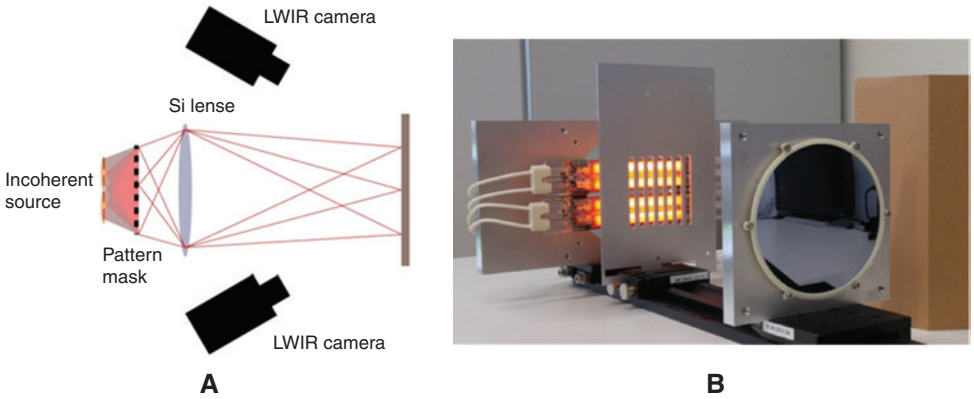

Figure 8: Experimental setup – incoherent source: (A) sketch of the experiment; (B) laboratory setup.

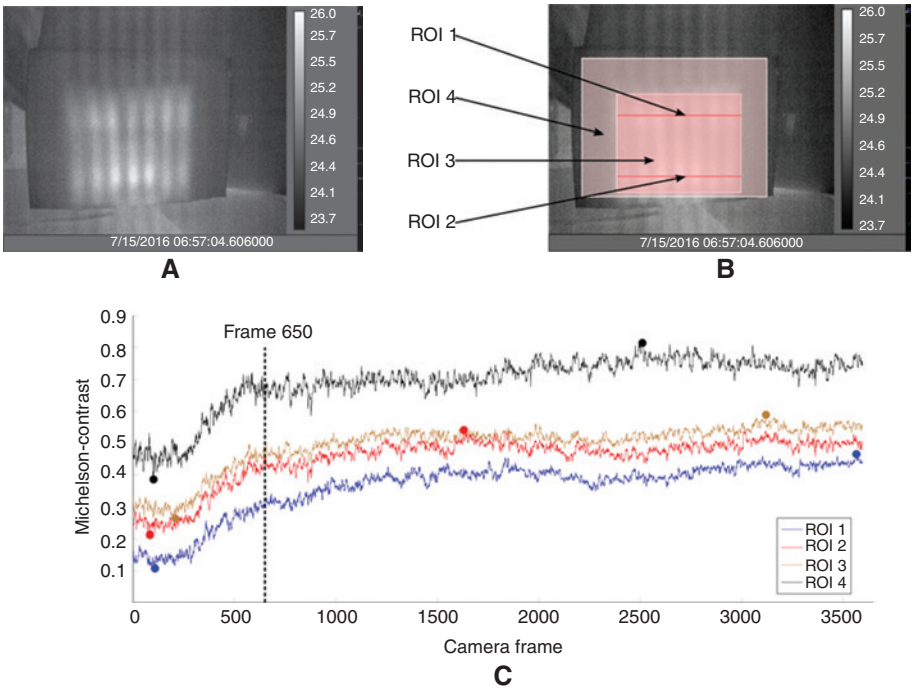

Figure 9: (A) Image from original video stream after 650 frames. (B) Four regions of interest indicated (ROI 1–ROI 4). (C) Contrast ratio for each region of interest plotted over 3600 frames. Maxima and minima are indicated as dots.

sizes were set to compute the normalized contrast ratio (Michelson-Contrast ratio) for each roi over time. The plot in Figure 9 indicates that after 650 video frames, the contrast ratio will not increase anymore. The 60 Hz frame rate equals 10.8 s. The plot also indicates that the contrast ratio will not decrease, not even after 60 s of constant radiation. That means that the energy from the pattern projection is small enough that the heat transfer inside the object does not influence the pattern contrast.

To conclude about the quality of 3D reconstruction data, further investigations have to be achieved first. For a first try using incoherent heat sources, the results look promising, even though the systems overall response time is fairly slow in comparison to the GOBO system.

5 Conclusion

In conclusion, we have shown two promising approaches for thermal 3D measurements of materials that cannot be measured in the visible wavelength range due to their transparency, absorption, translucence, or reflectivity.

One system operates with two MWIR cameras (3–5 µm) and a coherent high power CO_2 laser as heat source to introduce heat patterns onto the object surfaces. The heat patterns were generated with a GOBO wheel made of steel, which withstands the heat of the laser and offers the opportunity for faster measurements, in the future. Three parameters were varied to characterize the system and to understand their relationships. Therefore, the flatness error of a granite plate was determined where we fitted the reconstructed 3D points to a plane and extracted the standard deviation values. As a result, it was shown that there is a context between the rotation of the wheel, the exposure time, and the time when the images were taken. With the actual setup, we achieved a minimum flatness error of about 150 µm at 500-ms exposure time and at 20% rotation, which correlates to the movement of the middle stripe period. Further experiments are required in the future where we want to optimize the GOBO wheel and analyze the relationships of thermal contrasts and reconstruction results without a certain cooling period during the measurements.

Additionally, we experimented with a second system that used an incoherent heat source to investigate if there is a chance to provide a heat pattern-based 3D restoration system that not utilizes high-power laser sources. A low-budget setup was built. In contrast to the high speed GOBO system, it seems to be possible to use incoherent light sources to achieve the task but with several drawbacks. One is the long measurement time it takes to provide sufficient image contrast for reconstruction. On the other hand, the energy density limits the range of

materials to measure. The incoherent setup benefits when security and health regulations prohibit open high-power laser sources. The evaluation of the quality of these 3D point cloud results by triangulation using incoherent heat pattern requires further research work.

Acknowledgments: The part of this research at Ilmenau University of Technology was supported by the German Federal Ministry of Education and Research (BMBF) under grant no. 03ZZ0422.

References

[1] J. Geng, Adv. Opt. Photon. 3, 2 (2011).
[2] H. Nguyen, D. Nguyen, Z. Wang, H. Kieu and M. Le, Appl. Opt. 54, A9–A17 (2015).
[3] M. Schaffer, M. Grosse, B. Harendt and R. Kowarschik, Opt. Lett. 36, 16 (2011).
[4] S. Heist, P. Lutzke, I. Schmidt, P. Dietrich, P. Kühmstedt, et al., in Proc. SPIE 9868, 98680F (2016).
[5] P. Lutzke, P. Kühmstedt and G. Notni, Proc. SPIE 8493, 84930U (2012).
[6] I. Ihrke, K. N. Kutulakos, H. Lensch, M. Magnor and W. Heidrich, Comput. Graph. Forum 29, 2400–2426 (2010).
[7] G. Eren, O. Aubreton, F. Meriaudeau, L. A. S. Secades, D. Fofi, et al., Opt. Express 17, 14 (2009).
[8] O. Aubreton, A. Bajard, B. Verney and F. Truchetet, Mach. Vision Appl. 24, 7 (2013).
[9] E. Wiedenmann, M. Afrough, S. Albert, R. Schott, J. Tusch, et al., in Proc. SPIE 9525, 952514 (2015).
[10] A. Brahm, C. Rößler, P. Dietrich, S. Heist, P. Kühmstedt, et al., Proc. SPIE 9868, 98680C (2016).
[11] J. H. Lienhard IV and J. H. Lienhard V, in 'A Heat Transfer Textbook', (Dover Publications, Inc, Mineola, New York, 2011).
[12] Z. Zhang, IEEE Trans. Pattern Anal. Mach. Intell. 22, 1330–1334 (2000).
[13] S. Prakash, P. Y. Lee, T. Caelli and T. Raupach, Proc. SPIE 6205, 62050J (2006).
[14] S. Heist, P. Kühmstedt, A. Tünnermann and G. Notni, Opt. Eng. 55, 2 (2016).
[15] S. Heist, P. Lutzke, I. Schmidt, P. Dietrich, P. Kühmstedt, et al., Opt. Laser Eng. 87, 90–96 (2016).
[16] C. Bräuer-Burchardt, M. Heinze, I. Schmidt, P. Kühmstedt and G. Notni, Sensors 16, 1 (2015).